Check for updates

pH-Responsive Pickering emulsion stabilized by polymer-coated silica nanoaggregates and applied to recyclable interfacial catalysis†

Ruidong Luo, [ID] Jinfeng Dong and Yunbai Luo [ID] *

We first synthesized a diblock copolymer poly[tert-butyl methacrylate]-b-poly[3-(trimethoxysilyl)propyl methacrylate] (PtBMA-b-PTMSPMA) through reversible addition–fragmentation chain transfer (RAFT) living radical polymerization and grafted it onto fumed silica by converting the PTMSPMA segment to silanol and the PtBMA segment to polymethylacrylic acid (PMAA) in the presence of trifluoroacetic acid in order to obtain PMAA brush-coated silica nanoaggregates P-Si. TEM, DLS, FTIR, and TGA results confirmed the successful modification of the starting materials. The nanoaggregates flocculated and stabilized a toluene-in-water Pickering emulsion at low pH, while the nanoaggregates were well dispersed in water and broke the emulsion under both neutral and basic conditions. Alternatively, the addition of acid/base induced emulsification/demulsification cycles that were sustained for several cycles. Moreover, when the P-Si was mixed with Rh-loaded silica, Rh-Si, the mixture had the same pH-responsive Pickering emulsion behavior as the single P-Si. This Pickering emulsion system can be used in the biphasic interfacial catalytic hydrogenation of olefins and had excellent yields under a hydrogen atmosphere. The yield of Pickering emulsion catalysis rapidly reached more than 99% in 3 h, while that of the demulsified mixture failed to reach 20% in 4 h, which verified the promotion of catalysis by the Pickering emulsion. Base-induced demulsification can be used to separate the products and recycle the catalyst. This pH-responsive Pickering emulsion catalytic system was capable of several cycles of reuse, and there was no significant decrease in catalytic efficiency even after eight cycles.

1   Introduction

Pickering emulsions are biphasic systems in which droplets are stabilized by nanoparticles instead of environmentally harmful surfactants.[1,2] Because of the irreversible adsorption of nanoparticles at the oil–water interface,[3] Pickering emulsions are highly stable and offer many opportunities for a variety of applications, such as multifunctional materials,[4] oil recovery,[5] etc. In some applications, such as Pickering emulsion interfacial catalysis and controllable encapsulation and release of cargoes, a permanent and stable Pickering emulsion is not needed, and breaking the emulsion is complicated and energy-consuming. Thus, using an easy means of breaking the emulsion or reversing the phase of the emulsion, such as an outer stimulus, is important.

Stimuli-responsive Pickering emulsions have been well developed in recent decades,[6] and many stimuli, including CO_2/N_2,[7–11] pH,[12–19] temperature,[20–25] redox reduction,[26] light,[27–29] and double stimuli,[30–36] have been used to induce the demulsification or phase inversion of Pickering emulsions. Manipulating the pH by alternately adding acid or base to the system is simple and easy to implement. Though salts are generated and will accumulate in the system, these are not harmful to the environment. Moreover, compared to pH-responsive Pickering emulsions, modifying nanoparticles in order to obtain other stimuli-responsive Pickering emulsions is too complicated and not that common.

Yang was the first to use these stimuli-responsive properties to promote Pickering emulsion interfacial catalysis.[37] In the latter, the formation of the emulsion increases the oil–water contact area, and thus accelerates the reaction rate of biphasic catalysis.[38] However, following the reaction, separation of the catalytic products and recycling of the catalyst are also needed. Thus, stimuli-responsive Pickering emulsions offer a way to break or reverse the emulsion in order to make the above goals easier to achieve. Many stimuli, including pH,[37,39–41] CO_2/N_2,[42] light,[29] temperature,[43] and double stimuli,[44] have been used to isolate the product and recycle the catalyst. Among these, varying the pH is rapid and easy to manipulate, and thus an attractive method for designing a recyclable Pickering emulsion catalyst system.

In this study, we have built a pH-responsive Pickering emulsion system that was stabilized by polymer-coated silica

nanoaggregates, P-Si, and the properties of the emulsion were fully characterized. The nanoaggregates flocculated at low pH values and were able to stabilize the Pickering emulsion, while they dispersed in water under neutral and basic conditions and prevented the emulsion from forming. Thus, the system could be switched from emulsification to demulsification by alternately adding acid or base to the system many times. Moreover, fumed silica-loaded Rh had the same pH-responsive behavior when mixed with the nanoaggregates P-Si, even though it was unable to stabilize the emulsion alone. The Pickering system, which greatly increased the oil–solid contact area, could be used for the hydrogenation of alkenes when the reactant was added to the oil phase and hydrogen was bubbled through the system. The system was demulsified and separated into two phases with the addition of base, while the oil phase, containing product, could be isolated and the aqueous phase, containing nano-catalyst, could be recycled for further Pickering emulsion catalysis. Thus, these experiments have confirmed that pH-responsive Pickering emulsions stabilized by polymer-coated silica nanoaggregates provide a rapid means of recovering catalytic products and catalysts, and might therefore find wider application in the future.

2 Experimental

2.1 Materials

Fumed silica (HL-200) with a primary diameter of approximately 20 nm was provided by Guangzhou GBS High-Tech and Industry Co., Ltd (Guangzhou, China). The RAFT agent 2-cyano-2-propyl benzodithioate (CPDB) was synthesized according to the procedure described in the literature.[45] The monomer *tert*-butyl methacrylate (tBMA, 99%) and 3-(trimethoxysilyl)propyl methacrylate (TMSPMA, 97%) were purchased from Aladdin Industrial Corporation (Shanghai, China). The initiating agent, 2,2′-azobis(2-methylpropionitrile) (AIBN), was recrystallized twice from ethanol before use. Toluene (99.5%) was purchased from Aladdin. Trifluoroacetic acid (TFA, 99%) and rhenium trichloride hydrate (RhCl$_3$·3H$_2$O, 99%) was purchased from Energy-chemical Corporation (Shanghai, China). Sodium borohydride (NaBH$_4$, 96%) was purchased from Sinopharm Group Co., Ltd (Beijing, China). Ultrapure water was generated from a Milli-Q® Ultrapure Water System.

2.2 Synthesis of the PtBMA-*b*-PTMSPMA diblock copolymer

The diblock copolymer poly[*tert*-butyl methacrylate]-*b*-poly[3-(trimethoxysilyl)propyl methacrylate] (PtBMA-*b*-PTMSPMA) was synthesized by a typical RAFT living radical polymerization, as described below.

2.2.1 Synthesis of PtBMA macro-CTA. tBMA (14.2 g, 100 mmol), CPDB (0.221 g, 1 mmol), AIBN (0.041 g, 0.25 mmol), and CHCl$_3$ (40 mL) were added to a Schlenk tube and bubbled with N$_2$ gas for more than 20 min to expel the air. The reaction was conducted at 60 °C for 12 h. The final red powder, PtBMA macro-CTA was purified by being precipitated three times from a mixture of methanol and water (v/v = 7/3).

2.2.2 Synthesis of the diblock copolymer PtBMA-*b*-PTMSPMA. PtBMA macro-CTA (11.5 g, 1.07 mmol), TMSPMA (3.81 g, 15.36 mmol), AIBN (0.037 g, 0.23 mmol), and CHCl$_3$ (50 mL) were added to a Schlenk tube and bubbled with N$_2$ gas for more than 20 min to expel the air. The reaction was conducted at 60 °C for 12 h. The final red powder product, PtBMA-*b*-PTMSPMA, was purified by being precipitated three times from a mixture of methanol and water (v/v = 7/3).

2.3 Synthesis of polymer-coated silica nanoaggregates

Fumed silica was coated with the PtBMA-*b*-PTMSPMA polymer in toluene using TFA as catalyst.

Typically, 2.0 g fumed silica was ultrasonicated for 5 min in 200 mL toluene to disperse the nanoparticles. Subsequently, 0.5 g PtBMA-*b*-PTMSPMA was added under stirring. After stirring for 30 min, 2 mL TFA was added to catalyze the reaction. During the reaction, the PTMSPMA segment was changed to silanol by acidolysis of TFA and then reacted and grafted onto the fumed silica. The PtBMA segment changed to poly-methylacrylic acid (PMAA) by acidolysis of TFA. Thus, PMAA-coated silica was finally achieved. The particles were made to settle out by means of centrifugation at 12 000 rpm for 10 min and purified by being redispersed in ethanol and settled out again by centrifugation. This dispersion–centrifugation–dispersion procedure was repeated three times to remove any excess polymer. The final product (pink powder) was dried under vacuum at 120 °C for 2 h and denoted as P-Si; the synthesis of P-Si is shown in Scheme 1.

2.4 Synthesis of Rh-loaded silica

Rh-loaded silica was obtained by wet reduction of Rh(III). Typically, 0.5 g fumed silica was well dispersed in 50 mL water by ultrasonic treatment. Then, RhCl$_3$·3H$_2$O (0.0128 g, 0.048 mmol) was added and the mixture stirred for 4 h. Next, aqueous NaBH$_4$ solution (0.0073 g, 0.193 mmol, dissolved in 5 mL water) was added dropwise to the dispersion under rapid stirring and reacted overnight. Following the reaction, the resulting black powder was isolated by means of centrifugation and was washed with water four times to ensure no small molecules remained. The final loading of Rh was 0.88 wt% for the mixture as determined by inductively coupled plasma atomic emission spectroscopy (ICP-AES), and this Rh-loaded silica was denoted as Rh-Si.

Moreover, different amount of RhCl$_3$·3H$_2$O were used here, and the corresponding loading of Rh were 0.41 wt% and 1.82 wt%.

2.5 Characterization of the polymer and nanoparticles

2.5.1 Characterization of the polymer. The diblock copolymer was characterized by ^{1}H NMR (400 MHz Bruker Avance-400 spectrometer, Bruker BioSpin Corporation, Billerica, MA, USA) and gel permeation chromatography (GPC) measurements (Wyatt GPC instruments, Wyatt Technology Corporation, Santa Barbara, CA, USA). The corresponding figures are shown in the ESI† and the diblock copolymer can be expressed as PtBMA$_{74}$-*b*-PTMSPMA$_{17}$ based on the characterization.
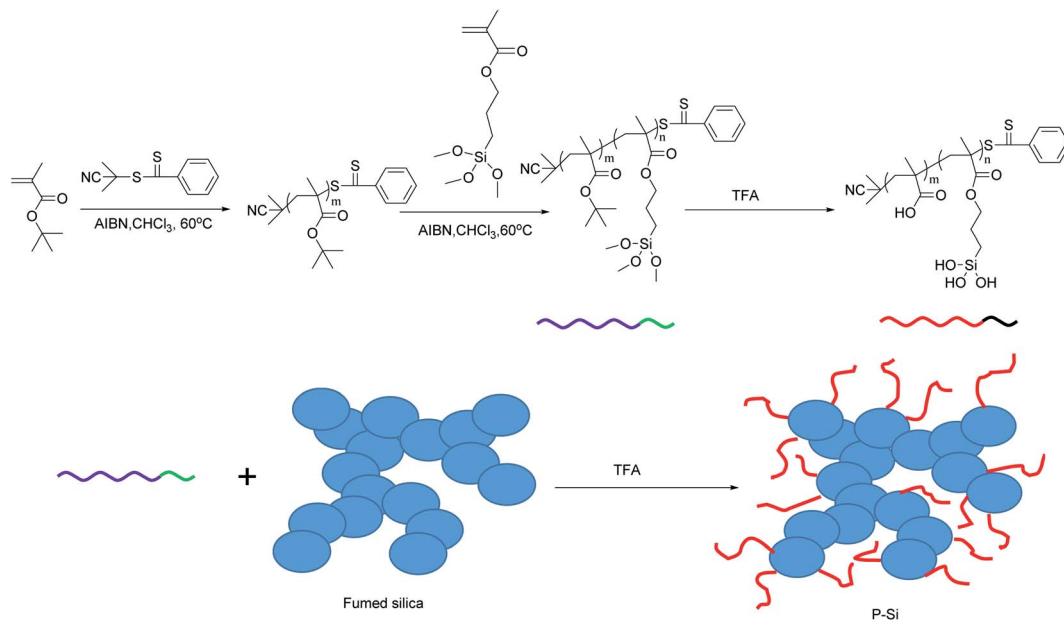
Scheme 1 Synthesis of the diblock copolymer PtBMA-*b*-PTMSPMA and P-Si.

2.5.2 Dynamic light scattering (DLS). The hydrodynamic diameters of the fumed silica, P-Si, and Rh-Si and the zeta potential of the P-Si at different pH values were measured using a Malvern Zetasizer Nano ZS (Malvern Panalytical Ltd, Malvern, UK).

2.5.3 Thermogravimetric analysis (TGA). TGA of the fumed silica and P-Si was performed on a NETZSCH TG 209 F1 instrument (NETZSCH TAURUS Instruments GmbH, Weimar, Germany) using air as the heating atmosphere. A typical measurement involved heating a sample from room temperature to 800 °C at a rate of 10 °C min^{-1}.

2.5.4 Transmission electron microscopy (TEM). TEM images of fumed silica, PMAA-Si, and Rh-Si were obtained on a JEM-2100 transmission electron microscope (JEOL, Tokyo, Japan).

2.5.5 Infrared spectrum (IR). The IR spectra of fumed silica and P-Si were recorded on a Thermo Scientific Fourier Infrared spectrometer (Thermo Scientific, Waltham, MA, USA).

2.5.6 Surface tension (SFT) and interfacial tension (IFT). The SFT of a P-Si dispersion (1.0 wt%) at different pH values was measured using the plate method on a Krüss K100 surface tension meter (KRÜSS GmbH, Hamburg, Germany). The IFT between the
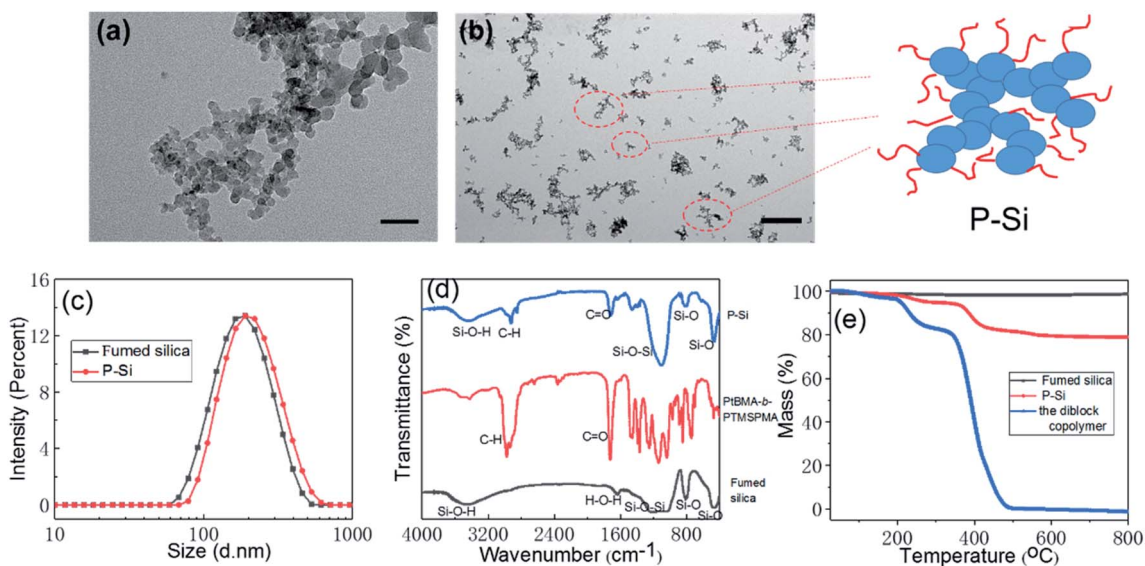

Fig. 1 (a) A TEM image of fumed silica, the scale bar: 100 nm; (b) a TEM image of P-Si, the scale bar: 500 nm; (c) DLS results of fumed silica and P-Si; (d) FTIR results of the diblock copolymer, fumed silica and P-Si; (e) TG results of fumed silica, P-Si and the diblock copolymer PtBMA$_{74}$-*b*-PTMSPMA$_{17}$.
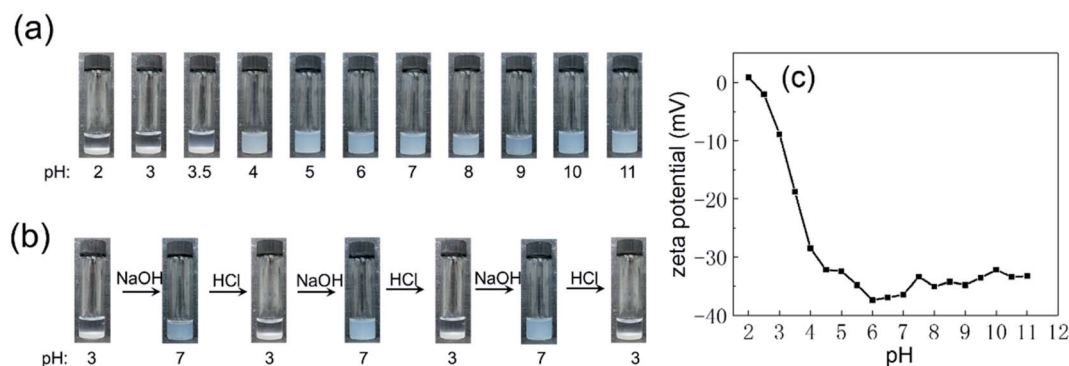
Fig. 2 (a) Images of P-Si aqueous dispersions at different pH values; (b) cycle of flocculation and dispersion of P-Si under the stimulus of acids/bases; (c) zeta potential of P-Si at different pH values.

same dispersion and toluene was measured using the pendant drop method on a Krüss DSA100 drop shape analyzer.

2.5.7 Contact angle. The contact angles of water (pH 3 and 9) on the nanoparticles were measured using the sessile drop method on a Krüss DSA100 drop shape analyzer.

2.6 Preparation and characterization of Pickering emulsions

The nanoparticle aqueous dispersions (different concentrations, different pH values) were mixed with a toluene phase of the same volume, and then the mixture was emulsified by means of vigorous hand shaking or homogenization (13 500 rpm, 2 min) using an IKA ULTRA-TURRAX T 25 homogenizer (IKA® England Ltd, Oxford, UK). The emulsion droplets were observed and recorded using an Olympus BX51 microscope (Olympus Corporation, Tokyo, Japan), and the emulsion type was determined by means of a drop test.

2.7 Performance of the Pickering emulsion catalysis in the catalysis of hydrogenation

P-Si and Rh-Si (m/m = 1 : 1) were mixed together and dispersed into 2 mL water. The total concentration was set at 1.0 wt%, and NaOH and HCl was used to adjust the pH. A small volume of the toluene phase (2 mL) dissolved in an olefin (1 mmol) was used as the oil phase. A hydrogen atmosphere was provided by a balloon of hydrogen gas. Gas chromatography (GC-2010 Plus, Shimadzu, Kyoto, Japan) was used to measure the yield.

3 Results and discussion

3.1 Characterization of P-Si

To get a better understanding of P-Si, the raw material (fumed silica, HL-200) was characterized by TEM and DLS measurements (Fig. 1a and c). From the figure, it can be seen that the primary nanoparticles of fumed silica were approximately 20 nm in size, but there were no clear boundaries between the nanoparticles. The DLS results revealed that the hydrodiameter of the fumed silica was 188 nm (polydispersity index (PDI) = 0.104), which was much greater than the diameter of the primary nanoparticles. Thus, fumed silica nanoparticles became nanoaggregates because of their high surface energy, and the basic units of fumed silica that dispersed in water or were chemically modified were actually nanoaggregates. Thus, when the fumed silica was coated with the diblock copolymer PtBMA-b-PTMSPMA using the sol–gel method, the basic units that were chemically modified were the nanoaggregates, not the primary nanoparticles. As shown in Fig. 1b, the TEM sample was prepared using 0.01 wt% P-Si aqueous dispersion. Thus, the basic constituent units of the P-Si were the various-sized branched nanoaggregates of the primary nanoparticles. The DLS, FTIR, and TGA results confirmed the successful modification of the polymer on the nanoaggregates. As shown in Fig. 1c, the hydrodynamic diameter of the P-Si was about 205 nm (PDI = 0.132), a little larger than that of the fumed silica, which indicated that the polymer brush on the nanoaggregates
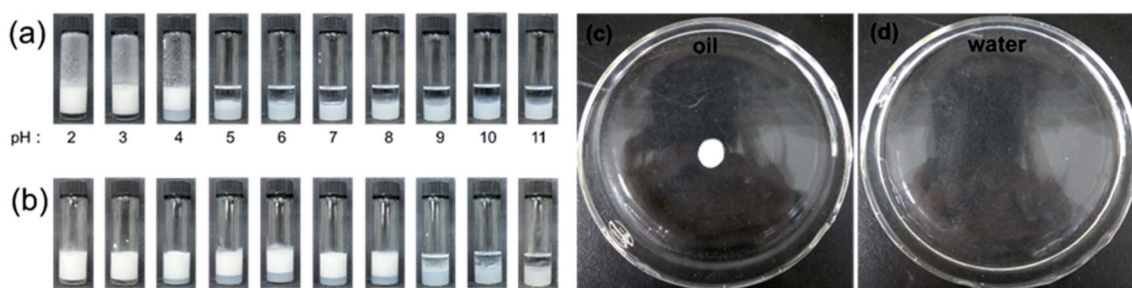

Fig. 3 Pickering emulsions prepared between PMAA-Si aqueous dispersion (1.0 wt%, different pH values, 2 mL) and toluene (2 mL). Emulsifying method: (a) vigorous hand-shaking; (b) homogenizing using an IKA ULTRA-TURRAX T 25 homogenizer (13 500 rpm, 2 min); (c) emulsion dropped into oil; (d) emulsion dropped into water.

increased the diameter. In the FTIR spectra of the polymer, the fumed silica, and the P-Si shown in Fig. 1d, the P-Si showed not only the characteristic peaks of silica but also those of the polymer: the bands at 2833–3040 cm^{-1} (C–H) and 1720 cm^{-1} (C=O) in the spectrum of PMAA-Si confirmed the successful modification. The TGA results in Fig. 1e indicate that the fumed silica did not show any apparent loss in weight, and TG curve of the diblock copolymer had a similar shape with that of the P-Si.

So the weight loss of the P-Si (about 19.24%) was belonged to the polymer grafted on the nanoaggregates.

The polymer brush on the P-Si was PMAA, which is a pH-responsive polymer. Thus, the effect of pH on the dispersion behavior of the P-Si in water was taken into consideration, as shown in Fig. 2a. The P-Si was well dispersed in water when the pH was above 4, and the P-Si flocculated at the bottom of the aqueous phase when the pH was no more than 4. Fig. 2c shows that the zeta potential of the P-Si was mostly between −30 and −40 mV when the pH was above 4, and so the nanoaggregates were able to be dispersed in water because of the electrostatic repulsion between them. The zeta potential approached 0 mV as the pH decreased, so that the P-Si flocculated. Moreover, Fig. 2b reveals that the P-Si was able to transform between the flocculated state and the dispersion state by alternately injecting acid or base several times to the dispersion. The pH-responsive dispersion behavior and the change in zeta potential of the P-Si was due to the pH-responsive protonation of the PMAA brush.

When the nanoparticles were able to stabilize the Pickering emulsion, the nanoparticles were amphiphilic and able to be adsorbed at the oil–water interface. As the results of the contact angle test shown in Fig. S2a and b† suggest, the sessile drop at different pH values had different contact angles. The contact angle at pH 3 was 46°, which meant that the P-Si was amphiphilic but biased toward being hydrophilic. The contact angle at pH 9 was 7°, which meant that the P-Si was extremely hydrophilic. The SFT and IFT data shown in Fig. S2† characterize the absorption of the P-Si at the surface of the aqueous dispersion and the toluene–water interface. The SFT and IFT values at pH values above 7 were about 71 and 30 mN m^{-1}, respectively, which were close to the SFT value of pure water and the IFT value of the pure water–toluene interface, respectively. Thus, the P-Si nearly failed to adsorb at the surface and the interface under these conditions. As the pH decreased, the SFT and IFT values decreased about 15 mN m^{-1}, which indicated that the P-Si was able to be adsorbed at the surface and the toluene–water interface at low pH. The contact angle, SFT, and IFT results all displayed the amphiphilicity of the P-Si and the possibility of the P-Si stabilizing Pickering emulsions at low pH values.

3.2 Characterization of the Pickering emulsion and its pH-responsive behavior

As has been described above, the P-Si showed pH-responsive dispersion behavior. Therefore, the emulsifying ability of the P-Si as a function of pH was tested using two different methods. As shown in Fig. 3, using vigorous hand-shaking as the first emulsifying method, the Pickering emulsion formed only at pH values no greater than 4. Furthermore, the remaining aqueous
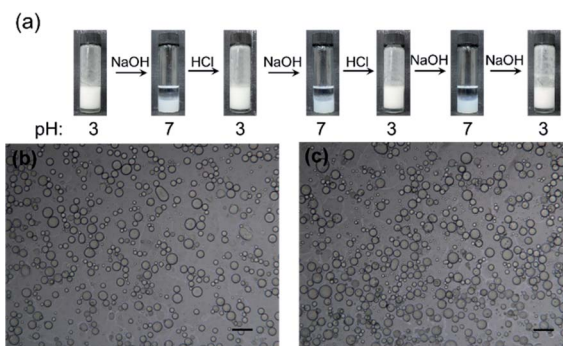

Fig. 4 (a) Cycles of emulsification and demulsification of PMAA-Si under the stimulus of acid/base; (b) image of Pickering emulsion droplets in the first cycle (scale bar: 100 μm); (c) image of Pickering emulsion droplets in the fourth cycle (scale bar: 100 μm).

phase still contained dispersed nanoparticles at pH 4, so the P-Si did not fully adsorb at the toluene–water interface to stabilize the emulsion. While the remaining aqueous phase was clear at pH 2 and 3, all of the nanoparticles were used to stabilize the emulsion.

A different set of emulsification results resulted when the mixture was emulsified using the homogenizer: the Pickering emulsion formed at pH 6–8, and the nanoparticles were dispersed in the corresponding remaining aqueous phase. The difference between the emulsification results might have resulted from the fact that the high-speed shearing probe of the homogenizer shattered the nanoaggregates into smaller pieces through the shearing force. Thus, in order to maintain the integrity of the P-Si nanoaggregates, vigorous hand-shaking was adopted as the emulsifying method in the following experiments. Moreover, the type of Pickering emulsion was oil-in-water, as determined by a drop test (Fig. 3c and d). An emulsion drop spread apart on water and remained as a white drop on oil, which indicated that the external phase of the Pickering emulsion was water.

A pH value of 3 was good for emulsification, as mentioned above. Thus, the effect of the concentration of the P-Si on the Pickering emulsion was taken into consideration when the pH was set to 3 and hand-shaking was used as the emulsifying method. As shown in Fig. S3a,† the Pickering emulsion formed at P-Si concentrations of 0.1–3.0 wt%, and the volume of the
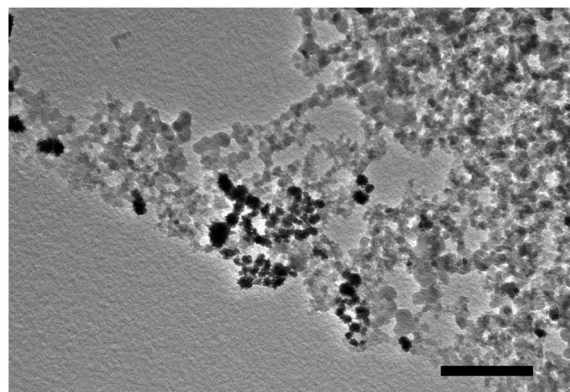

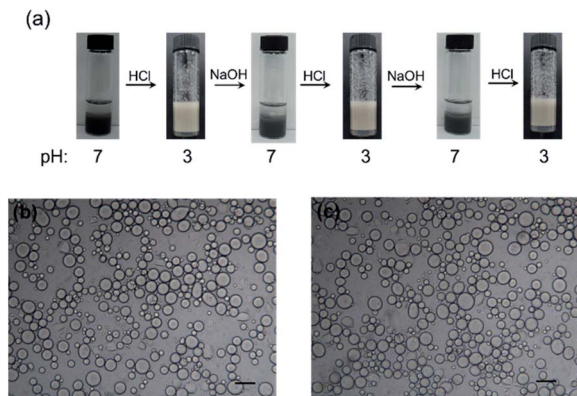Fig. 5 A TEM image of the Rh-Si (scale bar: 100 nm).

Fig. 6 (a) Cycles of emulsification and demulsification of a mixture of P-Si and Rh-Si under the stimulus of acid/base; (b) image of Pickering emulsion droplets in the first cycle (scale bar: 100 μm); (c) image of Pickering emulsion droplets in the fourth cycle (scale bar: 100 μm).

Pickering emulsion increased as the concentration of the P-Si increased. When determining the statistics of the diameter distribution of droplets on the images of Pickering emulsion droplets using the GuassAmp function, as shown in Fig. S3b and c,† the average diameter of Pickering emulsion droplets decreased as the concentration of the P-Si increased, and the distribution of diameters was correspondingly narrower. The diameter of Pickering emulsion droplets decreased rapidly when the concentration was lower than 1.25 wt% and decreased only slightly when the concentration was higher; the diameters of Pickering emulsion droplets were in the range 15–30 μm when the concentration of the P-Si was more than 1.5 wt%.

The pH-responsive behavior of the P-Si-stabilized Pickering emulsion is shown in Fig. 4a. The P-Si was dispersed in 2 mL water to get a concentration of 1.0 wt%, and the pH was adjusted to 3 with HCl to flocculate the nanoaggregates. An equal volume of toluene was added, and the mixture was emulsified by means of vigorous hand-shaking to form a Pickering emulsion. NaOH was then added to the emulsion to adjust the pH to approximately 7 with continued shaking. The emulsion rapidly and completely separated into two phases within a minute, and the emulsion droplets that had adhered to the wall of the vial disappeared. Subsequently, HCl was added to the dispersion to adjust the pH to 3, and a Pickering emulsion formed again with vigorous hand-shaking. These cycles of emulsification and demulsification of the Pickering emulsion by alternately adding acid or base could be sustained for several cycles. As shown in Fig. 4b and c, there was no significant change in the diameter of the emulsion droplets, thus displaying excellent pH-responsive behavior.

3.3 Enhanced catalysis of hydrogenation by the Pickering emulsion

To apply P-Si to Pickering emulsion catalysis, we first synthesized the Rh-loaded fumed silica, Rh-Si. A TEM image of the Rh-Si (loading of Rh was 0.88 wt%) is shown in Fig. 5. It can be seen that the black particles are Rh and the gray particles are the fumed silica. Thus, Rh was successfully doped and mixed into the fumed silica. When measuring the emulsifying ability of the Rh-Si, it was found that the Rh-Si was unable to stabilize the emulsion at any pH value, while the mixture of P-Si and Rh-Si (m/m = 1 : 1) had the same pH-responsive emulsifying behavior as the single P-Si. The pH-responsive behavior of a mixture of P-Si and Rh-Si (m/m = 1 : 1, total concentration of 1.0 wt%) is shown in Fig. 6a. When adjusting the pH to approximately 7 by adding NaOH, the system separated into two phases, while the upper layer was toluene and the lower black aqueous layer was a dispersion of P-Si and Rh-Si. Subsequently, the addition of HCl to adjust the pH to 3 and emulsifying the mixture by means of hand-shaking, a Pickering emulsion formed. From the images of this emulsion, the emulsion layer was found to be gray and the lower remaining aqueous phase was found to be transparent and colorless. Thus, all of the Rh-Si was located in the emulsion layer, and this would be helpful for Pickering emulsion catalysis. However, the diameters of the
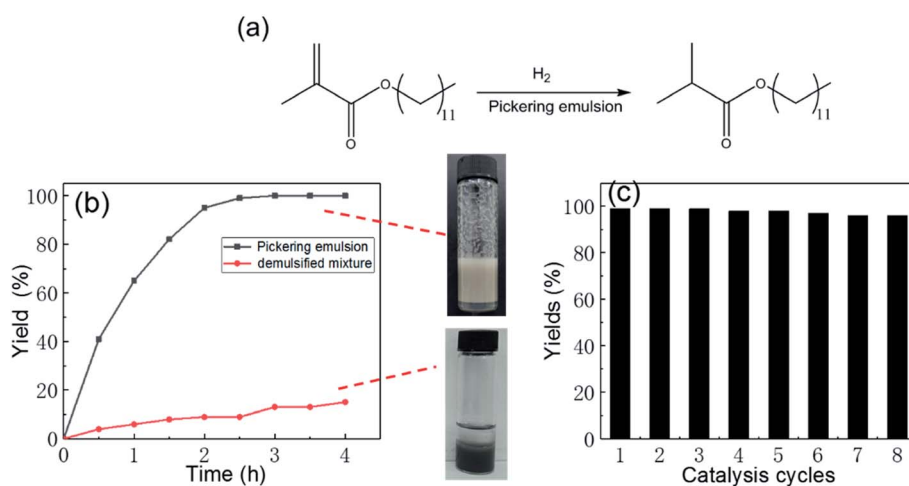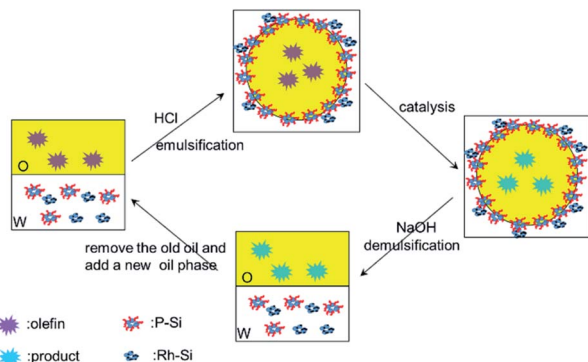

Fig. 7 (a) Enhanced catalysis of hydrogenation of lauryl methacrylate by the Pickering emulsion; (b) the yield of the Pickering emulsion catalysis and demulsified biphases at different times: the loading of Rh in Rh–Si was 0.88 wt% and the concentration of the mixture was 1.0 wt%; (c) the yield of Pickering emulsion catalysis over multiple catalytic cycles in 3 h.

Scheme 2 Catalytic cycles of a pH-responsive Pickering emulsion.

Pickering emulsion droplets stabilized by the mixture were slightly larger than those of the single P-Si (average diameters: 87 μm for the mixture and 67 μm for the single P-Si, the larger size of Pickering emulsion droplet was the result of the lower concentration of the effective emulsifying component – the P-Si). On adding NaOH to adjust the pH to 7 and shaking the vial for a while, the Pickering emulsion completely separated into two phases. Further addition of HCl to adjust the pH to 3 and emulsifying the mixture by means of hand-shaking led to the formation of a Pickering emulsion again. This pH-responsive behavior was sustained over several cycles. Fig. 6b and c shows that there were no significant changes in the Pickering emulsion droplets after several cycles of emulsification and demulsification. The reason why the Rh-Si was able to stabilize the emulsion together with the P-Si might be because the fumed silica can easily become aggregates, so that the Rh-Si flocculated together with the P-Si at pH 3, enabling the Rh-Si to adhere to the surface of the emulsion droplets, which were coated with the P-Si.

The Pickering emulsion was stabilized by nanoparticles, which thus greatly increased the contact area of the oil–water and oil–solid interfaces, which is beneficial for biphasic catalysis. In this Pickering emulsion system, the Rh-Si stabilized the Pickering emulsion together with the P-Si,

and thus the contact between the Rh-Si and the olefin in the toluene phase was greatly promoted. This system, in which P-Si was used to form Pickering emulsion and Rh-Si acted as catalyst, could enhance the catalysis of the hydrogenation of olefins under a hydrogen atmosphere. To verify this assumption, the catalysis of the hydrogenation of lauryl methacrylate was set as the model reaction, as shown in Fig. 7a. Two states of the mixture shown in Fig. 7 were used to compare the yield of the catalytic reaction as a function of time: the aqueous phase (2 mL) was a dispersion of a mixture of P-Si and Rh-Si, a hydrogen atmosphere was provided by means of a balloon of hydrogen gas, 1 mmol lauryl methacrylate was dissolved in 2 mL toluene, and the yield of the catalysis was determined by gas chromatography (GC). The results are shown in Fig. 6b. For the Pickering emulsion, the yield quickly increased to 43% in 0.5 h and reached more than 99% within 3 h. By contrast, the yield increased slowly and reached no more than 20% within 4 h in the case of the demulsified mixture. The comparison of the yields proved the catalytic enhancement by the Pickering emulsion, which resulted from the much larger area of the Rh-Si compared to the oil.

As was mentioned above in Fig. 6a, the Pickering emulsion displayed pH-induced emulsification/demulsification behavior. This property could be used to isolate a product and recycle the catalyst several times. As shown in Scheme 2, P-Si and Rh-Si co-stabilized the Pickering emulsion at pH 3 and were used to catalyze the hydrogenation of lauryl methacrylate under a hydrogen atmosphere. NaOH was added to adjust the pH to 7, and the emulsion completely separated into two phases, the upper toluene phase with the product being isolated through suction by a straw and the yield being determined by GC. A new toluene phase dissolved in lauryl methacrylate was added to initiate a new catalytic cycle. The results for several catalytic cycles are shown in Fig. 7c; the high activity of the Pickering emulsion catalyst was confirmed by a yield of greater than 95%, even after eight cycles. In summary, the pH-responsive Pickering emulsion exhibited an excellent effect on the recycling of catalyst and the isolation of product.
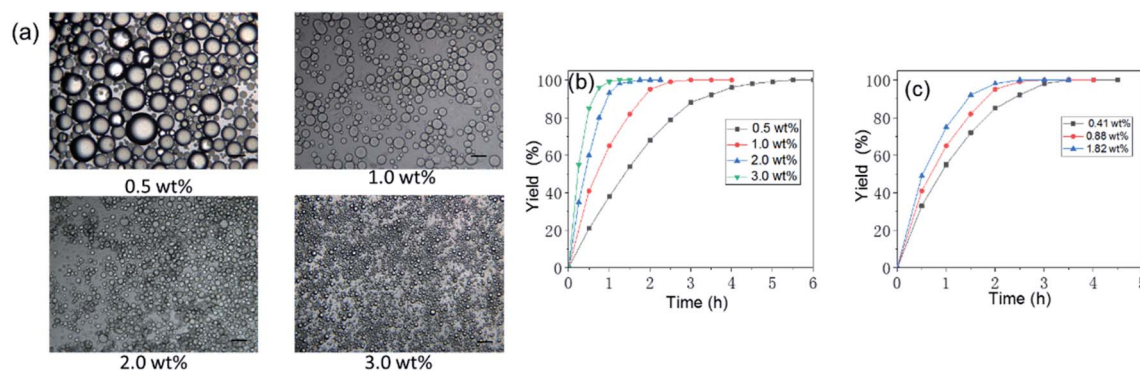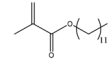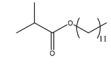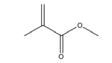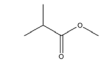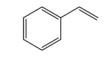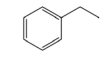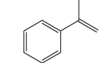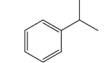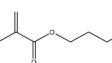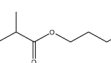

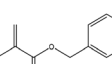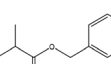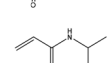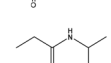Fig. 8   (a) Images of Pickering emulsion droplets (scale bar: 100 μm) stabilized by different concentration of a mixture of P-Si and Rh-Si (m/m = 1 : 1); (b) the yield of Pickering emulsion catalysis at different times: the loading of Rh in Rh–Si was 0.88 wt% and the concentration varied from 0.5 wt% to 3.0 wt%; (c) the yield of Pickering emulsion catalysis at different times: the concentration of the mixture was 1.0 wt% and the loading of Rh varied from 0.41 wt% to 1.82 wt%.

Table 1 Results of catalytic hydrogenation by means of the Pickering emulsion

Substrate	Product	t (h)	Yield (%)
		3	≥99
		2.5	≥99
		2	≥99
		2	≥99
		2.5	≥99
		3	≥99
		2.5	≥99

The concentration of the mixture of P-Si and Rh-Si and the loading of Rh in the Rh-Si were also taken into consideration. As shown in Fig. 8a and b, the size of Pickering emulsion droplets decreased as the concentration of the mixture went up, the corresponding speed of Pickering emulsion catalysis was accelerated. More specifically, the yield of hydrogenation of lauryl methacrylate reached more than 99% within 1 h when the concentration was 3.0 wt%, while the time needed to complete the catalysis was 5 h when the concentration was 0.5 wt%. The reason would be that the smaller Pickering emulsion droplets increased the contact area of oil phase and Rh-Si and thus accelerated the Pickering emulsion catalysis. As shown in Fig. 8c, different loading of Rh in Rh-Si was adopted in the Pickering emulsion catalysis, from the result, it could be found that high loading of Rh would increased the speed of catalysis but the degree of improvement was not as obvious as the decrease of the size of emulsion droplets. Specifically, the yield reached more than 99% within 2.5 h when the loading of Rh was 1.82 wt%, while time needed to complete the catalysis was 4 h when the loading of Rh was 0.41 wt%. In summary, for Pickering emulsion catalysis, the key to increase the catalytic rate was to decrease the size of emulsion droplets to increase the contact area; increasing the loading of Rh would increased the speed of catalysis but to a limited degree.

In addition, different kinds of olefins were adopted in this Pickering emulsion system to verify its wide applicability. Catalytic hydrogenation could run very well with different kinds of olefins, and the products are easily isolated. As shown in Table 1, different kinds of olefins, including styrene monomers, methacrylate monomers, and acrylamide monomers, had yields of more than 99% within 3 h in this Pickering emulsion catalytic system (the loading of Rh in Rh-Si was 0.88 wt% and the concentration of the mixture was 1.0 wt%), which is suitable for the catalytic hydrogenation of a wide range of olefins.

4   Conclusions

In this study, we have built a pH-responsive Pickering emulsion system stabilized by polymer-coated nanoaggregates, P-Si. The nanoaggregates flocculate and stabilize the toluene-in-water Pickering emulsion at low pH values, while the nano-aggregates are well dispersed in water and break the emulsion under neutral and basic conditions. These acid/base-induced emulsification/demulsification cycles can be sustained over several cycles. Moreover, when the P-Si is mixed with Rh-loaded silica, Rh-Si, the mixture has the same pH-responsive behavior as the single P-Si. This system can be used in the biphasic interfacial catalytic hydrogenation of olefins, and achieves yields of ≥99% under a hydrogen atmosphere. Base-induced demulsification can be used to separate the products and recycle the catalyst. This pH-responsive Pickering emulsion catalytic system can operate over multiple cycles, and there is no significant decrease in catalytic efficiency.

Conflicts of interest

There are no conflicts to declare.

Acknowledgements

References

1 S. U. Pickering, *J. Chem. Soc., Trans.*, 1907, **91**, 2001.
2 W. Ramsden, *Proc. R. Soc. London*, 1903, **72**, 156.
3 B. P. Binks, *Curr. Opin. Colloid Interface Sci.*, 2002, **7**, 21–41.
4 D. Yin, L. Ma, J. Liu and Q. Zhang, *Energy*, 2014, **64**, 575–581.
5 K. Y. Yoon, H. A. Son, S. K. Choi, J. W. Kim, W. M. Sung and H. T. Kim, *Energy Fuels*, 2016, **30**, 2628–2635.
6 J. Tang, P. J. Quinlan and K. C. Tam, *Soft Matter*, 2015, **11**, 3512–3529.
7 X. Yan, Z. Zhai, J. Xu, Z. Song, S. Shang and X. Rao, *J. Agric. Food Chem.*, 2018, **66**, 10769–10776.
8 Y. Shi, D. Xiong, Z. Li, H. Wang, Y. Pei, Y. Chen and J. Wang, *ACS Sustainable Chem. Eng.*, 2018, **6**, 15383–15390.
9 J. Jiang, Y. Zhu, Z. Cui and B. P. Binks, *Angew. Chem.*, 2013, **52**, 12373–12376.
10 C. Liang, Q. Liu and Z. Xu, *ACS Appl. Mater. Interfaces*, 2014, **6**, 6898–6904.
11 Y. Qian, Q. Zhang, X. Qiu and S. Zhu, *Green Chem.*, 2014, **16**, 4963–4968.
12 G. Ren, M. Wang, L. Wang, Z. Wang, Q. Chen, Z. Xu and D. Sun, *Langmuir*, 2018, **34**, 5798–5806.
13 S. Fujii, Y. Cai, J. V. M. Weaver and S. P. Armes, *J. Am. Chem. Soc.*, 2005, **127**, 7304–7305.

14 M. Motornov, R. Sheparovych, R. Lupitskyy, E. Macwilliams, O. Hoy, I. Luzinov and S. Minko, *Adv. Funct. Mater.*, 2007, **17**, 2307–2314.

15 J. Li and H. D. H. Stover, *Langmuir*, 2008, **24**, 13237–13240.

16 M. F. Haase, D. O. Grigoriev, H. Moehwald, B. Tiersch and D. G. Shchukin, *J. Phys. Chem. C*, 2010, **114**, 17304–17310.

17 J. Kim, L. J. Cote, F. Kim, W. Yuan, K. R. Shull and J. Huang, *J. Am. Chem. Soc.*, 2010, **132**, 8180–8186.

18 H. Liu, C. Wang, S. Zou, Z. Wei and Z. Tong, *Langmuir*, 2012, **28**, 11017–11024.

19 F. Tu and D. Lee, *J. Am. Chem. Soc.*, 2014, **136**, 9999–10006.

20 X. Pei, K. Zhai, C. Wang, Y. Deng, Y. Tan, B. Zhang, Y. Bai, K. Xu and P. Wang, *Langmuir*, 2019, **35**, 7222–7230.

21 Y. Zhu, T. Fu, K. Liu, Q. Lin, X. Pei, J. Jiang, Z. Cui and B. P. Binks, *Langmuir*, 2017, **33**, 5724–5733.

22 X. Wang, M. Zeng, Y. H. Yu, H. Wang, M. S. Mannan and Z. Cheng, *ACS Appl. Mater. Interfaces*, 2017, **9**, 7852–7858.

23 J. O. Zoppe, R. A. Venditti and O. J. Rojas, *J. Colloid Interface Sci.*, 2012, **369**, 202–209.

24 T. Saigal, H. Dong, K. Matyjaszewski and R. D. Tilton, *Langmuir*, 2010, **26**, 15200–15209.

25 B. P. Binks, R. Murakami, S. P. Armes and S. Fujii, *Angew. Chem.*, 2005, **44**, 4795–4798.

26 Q. Jiang, N. Sun, Q. Li, W. Si, J. Li, A. Li, Z. Gao, W. Wang and J. Wang, *Langmuir*, 2019, **35**, 5848–5854.

27 Y. Chen, Z. Li, H. Wang, Y. Pei, Y. Shi and J. Wang, *Langmuir*, 2018, **34**, 2784–2790.

28 R. Bai, L. Xue, R. Dou, S. Meng, C. Xie, Q. Zhang, T. Guo and T. Meng, *Langmuir*, 2016, **32**, 9254–9264.

29 Z. Chen, L. Zhou, W. Bing, Z. Zhang, Z. Li, J. Ren and X. Qu, *J. Am. Chem. Soc.*, 2014, **136**, 7498–7504.

30 C. Y. Xie, S. X. Meng, L. H. Xue, R. X. Bai, X. Yang, Y. Wang, Z. P. Qiu, B. P. Binks, T. Guo and T. Meng, *Langmuir*, 2017, **33**, 14139–14148.

31 J. Jiang, Y. Ma, Z. Cui and B. P. Binks, *Langmuir*, 2016, **32**, 8668–8675.

32 G. Ren, X. Zheng, H. Gu, W. Di, Z. Wang, Y. Guo, Z. Xu and D. Sun, *Langmuir*, 2019, **35**, 13663–13670.

33 J. Tang, R. Berry and K. C. Tam, *Biomacromolecules*, 2016, **17**, 1748–1756.

34 Y. Chen, Y. Bai, S. Chen, J. Ju, Y. Li, T. Wang and Q. Wang, *ACS Appl. Mater. Interfaces*, 2014, **6**, 13334–13338.

35 B. Brugger and W. Richtering, *Adv. Mater.*, 2007, **19**, 2973–2978.

36 J. Tang, M. F. X. Lee, W. Zhang, B. Zhao, R. Berry and K. C. Tam, *Biomacromolecules*, 2014, **15**, 3052–3060.

37 H. Yang, T. Zhou and W. Zhang, *Angew. Chem.*, 2013, **52**, 7455–7459.

38 M. Pera-Titus, L. Leclercq, J. M. Clacens, F. De Campo and V. Nardello-Rataj, *Angew. Chem.*, 2015, **54**, 2006–2021.

39 S. Wiese, A. C. Spiess and W. Richtering, *Angew. Chem.*, 2013, **52**, 576–579.

40 Z. Fang, D. Yang, Y. Gao and H. Li, *Colloid Polym. Sci.*, 2015, **293**, 1505–1513.

41 J. Huang and H. Yang, *Chem. Commun.*, 2015, **51**, 7333–7336.

42 S. Yu, D. Zhang, J. Jiang, Z. Cui, W. Xia, B. P. Binks and H. Yang, *Green Chem.*, 2019, **21**, 4062–4068.

43 B. Yao, Q. Fu, A. Li, X. Zhang, Y. Li and Y. Dong, *Green Chem.*, 2019, **21**, 1625–1634.

44 J. Tang, X. Zhou, S. Cao, L. Zhu, L. Xi and J. Wang, *ACS Appl. Mater. Interfaces*, 2019, **11**, 16156–16163.

45 M. Benaglia, E. Rizzardo, A. Alberti and M. Guerra, *Macromolecules*, 2005, **38**, 3129–3140.